Improvement in the mechanical properties and creep resistance of Al-Mn-Mg 3004 alloy with Sc and Zr addition

Zhen Li, Zhan Zhang, X.-Grant Chen *

Department of Applied Science, University of Quebec at Chicoutimi,
Saguenay, QC, Canada, G7H 2B1

Abstract

Sc and Zr were added to Al-Mn-Mg 3004 alloy to form two populations of strengthening particles (50–70 nm-sized α-Al(Mn,Fe)Si dispersoids and 6–8 nm-sized $Al_3(Sc,Zr)$ precipitates), and their strengthening effects on the mechanical properties and creep resistance at ambient and elevated temperatures were studied. The results showed that the microhardness and yield strength at ambient temperature greatly increased upon the addition of Sc and Zr. The creep resistance at 300 °C significantly improved due to the precipitation of fine $Al_3(Sc,Zr)$ particles and reduction of the particle-free zone. However, the yield strength at 300 °C remained constant even though the Sc and Zr content increased. The combined effects of α-Al(Mn,Fe)Si dispersoids and $Al_3(Sc,Zr)$ precipitates on the yield strengths at 25 °C and 300 °C were quantitatively analyzed based on the Orowan bypass and dislocation climb mechanisms. The analytically predicted yield strengths are in good agreement with the experimental data.

Keywords: Al-Mn-Mg 3004 alloy; α-Al(Mn,Fe)Si dispersoids; $Al_3(Sc,Zr)$ precipitates; Microstructure evolution; Mechanical properties; Creep resistance.

* Corresponding author – X.-Gant Chen, Tel: (418) 545-5011 ext. 2603; Fax: (418) 545-5012; Email: xgrant.chen@uqac.ca

1. Introduction

Al-Mn-Mg 3004 alloys are widely used in architecture, packaging and automobile industries, because of their excellent corrosion resistance and great workability. To achieve adequate mechanical properties, the 3004 alloys are generally strengthened by work hardening. Recently, dispersion strengthening has been found to be an effective method to strength AA3xxx alloys, particularly at elevated temperature [1-5]; in this case, α-Al(Mn,Fe)Si dispersoids act as the key strengthening phase. By appropriate heat-treatment, a large number of α-Al(Mn,Fe)Si dispersoids can be precipitated in the aluminum matrix of 3004 alloys and their volume fractions can be as high as 3% when the particles are in the size range of 40-80 nm [3]. In addition, α-Al(Mn,Fe)Si dispersoids are partially coherent with the aluminum matrix [6] and thermally stable up to 300 °C [3]. Although the size of α-Al(Mn,Fe)Si dispersoids is larger than those of traditional strengthening precipitates, such as Mg_2Si and Al_2Cu, the α-Al(Mn,Fe)Si dispersoids can efficiently be used for strengthening 3004 alloys at elevated temperature due to their large volume fractions and high thermal stability [3, 5], which are very attractive features for elevated temperature applications.

In several studies [7-9], Sc was introduced into aluminum alloys to enhance their mechanical properties by forming high density nano-scale Al_3Sc precipitates. Al_3Sc precipitates were coherent with the aluminum matrix and thermally stable up to 300 °C with a low coarsening rate [8]. Zr has often been added along with Sc, and it was found that Zr could substitute Sc in Al_3Sc to form $Al_3(Sc,Zr)$ precipitates [10]. $Al_3(Sc,Zr)$ precipitates exhibited better thermal coarsening resistance than Al_3Sc precipitates [10-12]. Due to the low solubility of Sc and Zr in aluminum, the obtainable volume fractions of the $Al_3(Sc,Zr)$ precipitates are usually low. However, the particle size of $Al_3(Sc,Zr)$ precipitates was quite small (a few nanometers) and their distribution was very uniform. As a result, the $Al_3(Sc,Zr)$ precipitates could improve the mechanical properties of aluminum alloys at both ambient and elevated temperatures. Therefore, Al-Sc-Zr matrices are considered promising candidates to develop materials to be used at elevated temperature.

In several other studies, Sc and Zr were introduced into conventional age-hardening aluminum alloys, such as AA2xxx, AA6xxx and AA7xxx alloys, to improve their mechanical properties [13-15]. The addition of Sc and Zr into AA2219 alloys was found to significantly

improve their hardness levels [13]. It was also observed that the tensile strength and high cycle fatigue limit of AA6106 alloys increased by alloying with Sc and Zr [14]; similarly, alloying with Sc and Zr increased the yield strength ofAA7xxx alloys [15]. The strength increase in AA2xxx, AA6xxx and AA7xxx alloys can be attributed to the combined action of aging precipitation strengthening phases (Al_2Cu, Mg_2Si and $MgZn_2$) and $Al_3(Sc,Zr)$ precipitates. Due to the rapid coarsening of Al_2Cu, Mg_2Si and $MgZn_2$ precipitates at elevated temperature (overage effect), most of the above cited studies focused on room-temperature mechanical properties. Hence, the advantages of alloying with Sc and Zr and precipitation of thermally stable $Al_3(Sc,Zr)$ were not fully utilized. Very little literature can be found on improving high-temperature mechanical properties by the synergetic effect of the two different types of strengthening phases.

The goal of the present work was to improve both ambient and elevated-temperature mechanical properties of 3004 alloy by introducing two distinct populations of strengthening particles: a high volume fraction of submicron α-Al(Mn,Fe)Si dispersoids and a low volume fraction of nano-size $Al_3(Sc,Zr)$ precipitates. The influence of Sc and Zr addition on the microstructure, mechanical properties and creep resistance at ambient and elevated temperatures was investigated. The combined effects of α-Al(Mn,Fe)Si dispersoids and $Al_3(Sc,Zr)$ precipitates on the yield strengths at 25 °C and 300 °C were quantitatively analyzed based on the existing strengthening mechanisms and equations. The analytically predicted yield strengths were then compared with the experimental data.

2. Experimental procedure

Three experimental 3004 alloys with different Sc and Zr contents were prepared with commercially pure Al (99.7%), pure Mg (99.9%), Al-25%Mn, Al-25%Fe, Al-50%Si, Al-2%Sc, and Al-15%Zr master alloys. In addition to the base alloy, the SZ15 and SZ30 alloys contained 0.18%Sc and 0.18%Zr and 0.29%Sc and 0.17%Zr, respectively. The chemical compositions of the experimental alloys analyzed by an optical emission spectrometer are listed in Table 1 (all the alloy compositions are indicated in wt.% unless otherwise mentined). For each batch, approximately 3 kg of the materials were melted in an electrical resistance furnace; the melt was held at 750 °C for 30 min and degassed for 15min.

It was then poured into a permanent steel mold preheated at 250 °C. The dimensions of the cast ingots was 30 mm x 40 mm x 80 mm.

Table 1 Chemical composition of experimental alloys (wt.%)

Code	Sc	Zr	Mn	Fe	Mg	Si	Al
SZ0 (base)	**0**	**0**	1.23	0.60	0.97	0.24	Bal
SZ15	**0.18**	**0.18**	1.18	0.59	1.04	0.25	Bal
SZ30	**0.29**	**0.17**	1.19	0.57	1.01	0.25	Bal

The three alloys were heat-treated with a heating rate 5 °C/min to 300 and 375 ℃ respectively, and then held at those temperatures for a time period varying between 2 h and 48 h, followed by water quenching. Heat treatment at 300 °C was used to evaluate the effect of Al_3(Sc,Zr) precipitates; at 300 °C only Al_3(Sc,Zr) can precipitate [16] because α-Al(Mn,Fe)Si dispersoids are not yet formed [3]. However, at 375 °C α-Al(Mn,Fe)Si dispersoids can fully precipitate in addition to the precipitation of Al_3(Sc,Zr).

After polishing the samples, their Vicker hardness values were measured with a 200g load at a 20s dwelling time. Ten measurements were conducted to calculate the average hardness value of each sample. Compression yield strength tests were conducted at room temperature and elevated temperature (300 °C) using a Gleeble 3800 thermomechanical testing unit at a strain rate of 0.001 s^{-1}. The Gleeble samples were machined in a cylinder form of 15 mm high and 10 mm diameter. Average results were obtained from three repeated tests. Creep tests were performed at 300 °C for 96 h in a compression condition with different loads of 44 MPa, 52 MPa, 58 MPa and 66.5 MPa, respectively. Each creep test was repeated twice. The creep specimens were the same size as the Gleeble samples.

An optical microscope and a scanning electron microscope were used to observe the as-cast and heat-treated microstructures. To clearly observe α-Al(Mn,Fe)Si dispersoids and dispersoid free zone (DFZ), the polished samples were etched by 0.5% HF for 25 s. A transmission electron microscope (TEM) operating at 200 kV was used to observe the precipitation of Al_3(Sc,Zr) and α-Al(Mn,Fe)Si. TEM foils were prepared by a twin-jet

machine using a solution of 30% nitric acid in methanol at -25 °C. For $Al_3(Sc,Zr)$ observation, centered dark field images of the precipitates were formed using the {100} superlattice reflections of precipitates along the <110> or <100> zone axis. For α-Al(Mn,Fe)Si observation, the <100> zone axis was used to observe dispersoid precipitation in the {200} plane. An electron energy loss spectroscopy (EELS) attached to the TEM was used to measure the thickness of the TEM specimens. The size, number density and volume fraction of the $Al_3(Sc,Zr)$ precipitates and α-Al(Mn,Fe)Si dispersoids were quantified by image analysis (Clemex PE 4.0) of the TEM images. The volume fraction of the α-Al(Mn,Fe)Si dispersoids was calculated using the following equation [1]:

$$V_v = A_A \frac{K\bar{D}}{K\bar{D} + t}(1 - A_{DFZ}) \quad (1)$$

Where A_A is the area fraction of dispersoids in TEM images and $\bar{D}$ is the average equivalent diameter of dispersoids in TEM images; A_{DFZ} is the volume fraction of DFZ measured in optical images; t is the TEM foil thickness; and K is the average shape factor of dispersoids, which was set to 0.45 according to reference [1].

3. Results and discussion

3.1 Microstructures in as-cast and heat-treated conditions

Fig. 1 shows the typical as-cast microstructure of the three experimental alloys; it can be seen that the microstructures consist of aluminum dendrite cells and two intermetallic phases. The first type of intermetallics are grey color appeared under optical microscope; they are distributed in the aluminum dendrite boundaries. Most of them were identified as $Al_6(Mn,Fe)$ and very few of them identified as Al(Mn,Fe)Si [3, 4, 17]. Due to their similarities and no influence on alloy properties, this kind of intermetallics are referred to as Mn-containing intermetallics in this study. The second type of intermetallics are black color under optical microscope; they correspond to a minor phase identified as primary Mg_2Si, which is often attached to Mn-containing intermetallics. The volume fractions of both the intermetallic phases were quantified by image analysis, as shown in Fig. 2. The volume fractions of Mn-containing intermetallics and primary Mg_2Si particles in the base alloy were the lowest. With increasing Sc and Zr content, the fractions of both Mn-containing intermetallics and

primary Mg_2Si particles increased. It was reported that the addition of Sc and Zr could reduce the solubility of Mg and Mn in liquid aluminum [7, 18]. This is most likely the reason behind the remarkable increase in the amounts of Mn-containing intermetallics and primary Mg_2Si particles in the as-cast microstructure after Sc and Zr addition. Both SZ15 and SZ30 contain the same level of Zr but SZ30 exhibits a higher Sc level. This indicates that the increased amount of Sc could further reduce the solubility of Mg and Mn and thus increase the amount of intermetallic particles in the as-cast microstructure.

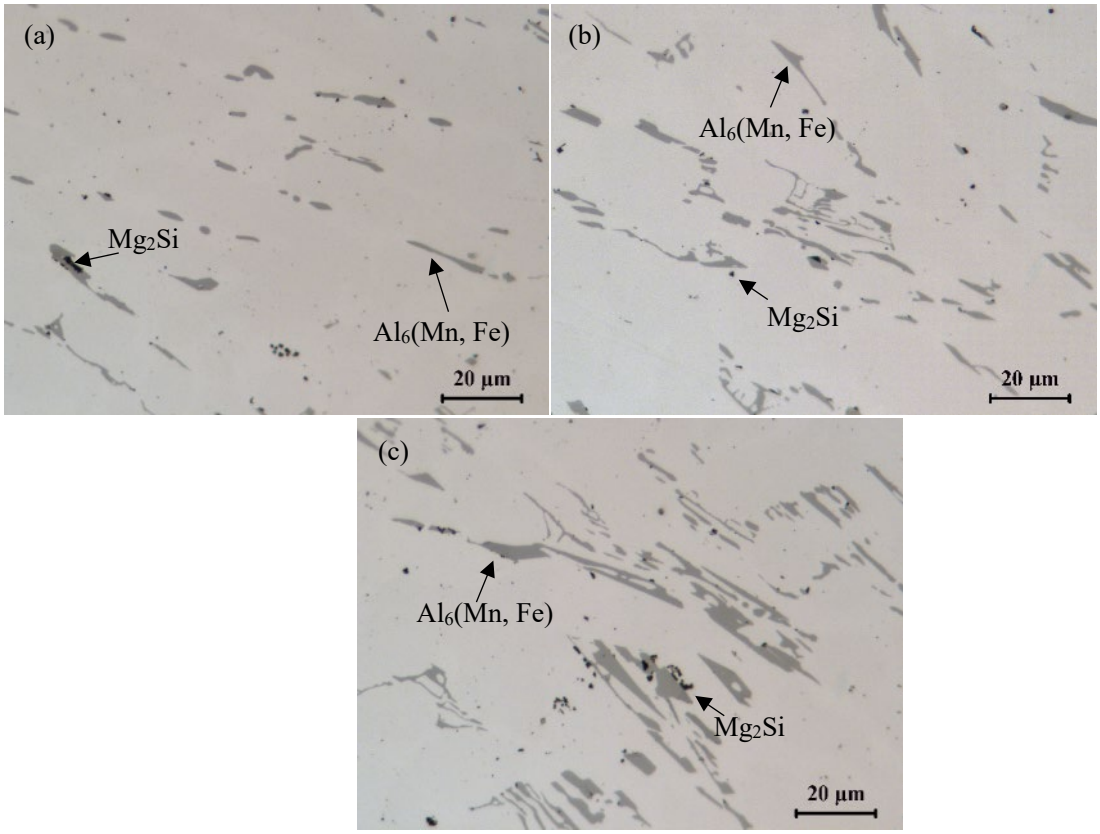

Fig. 1 As-cast microstructure of (a) SZ0, (b) SZ15 and (c) SZ30 alloys

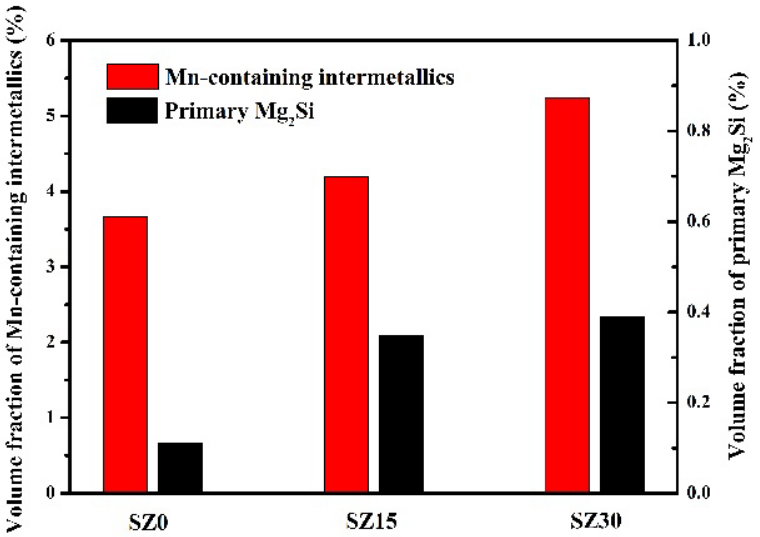

Fig. 2 Volume fraction of Mn-containing intermetallics and primary Mg_2Si particles of three alloys

In AA3004 alloys, a large amount of α-Al(MnFe)Si dispersoids can precipitate in the aluminum matrix when a suitable heat-treatment is applied, such as heat-treated at 375 ℃ for 24 h [3-5]. Fig. 3 depicts the microstructures of the three alloys after heat treatment at 375 °C for 24 h. The dark areas indicate the dispersoid zone in which a large number of α-Al(Mn,Fe)Si dispersoids appeare within dendrite cells and grains. The light areas correspond to the dispersoid free zone (DFZ) close to the intermetallic particles in the interdendritic regions. where only a few α-Al(Mn,Fe)Si dispersoids could be found. As shown in Fig. 3, with increasing Sc and Zr content, the dispersoid zones gradually decreased in size while the DFZs were enlarged. Quantitative results of both the dispersoid zone and DFZ, obtained by image analysis, are included in Fig. 4. It is evident that as the Sc and Zr content increases, the volume fraction of the dispersoid zone decreased while the volume fraction of the DFZ increased. For instance, the volume fraction of DFZ increased from 29 vol.% in the base alloy (SZ0) to 34 vol.% in the SZ15 alloy, and further to 38 vol.% in the SZ30 alloy.

It should be mentioned that the optical images of the microstructure obtained after etching can only be used to evaluate the distribution of α-Al(Mn,Fe)Si dispersoids, and it cannot reveal any information on the $Al_3(Sc,Zr)$ precipitates due to their small sizes (nanometric order).

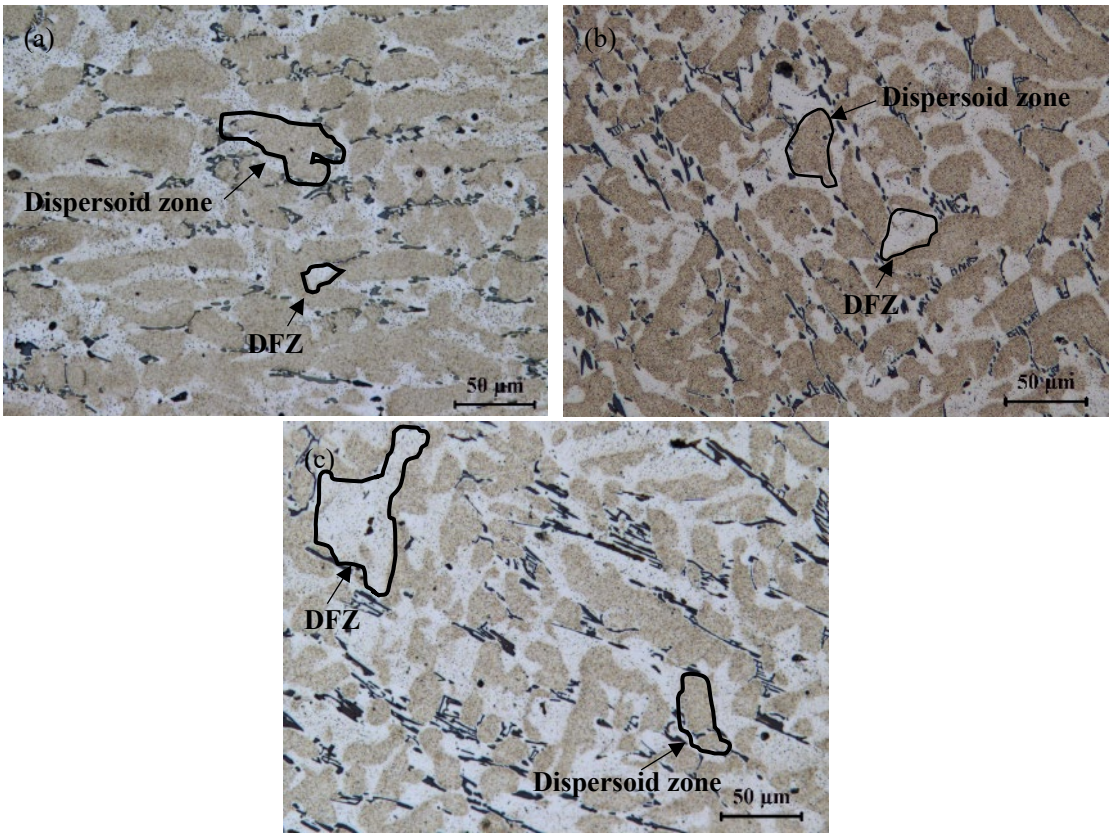

Fig. 3 Optical images after heat treatment at 375°C/24h (etched by 0.5% HF): (a) SZ0, (b) SZ15 and (c) SZ30 alloys

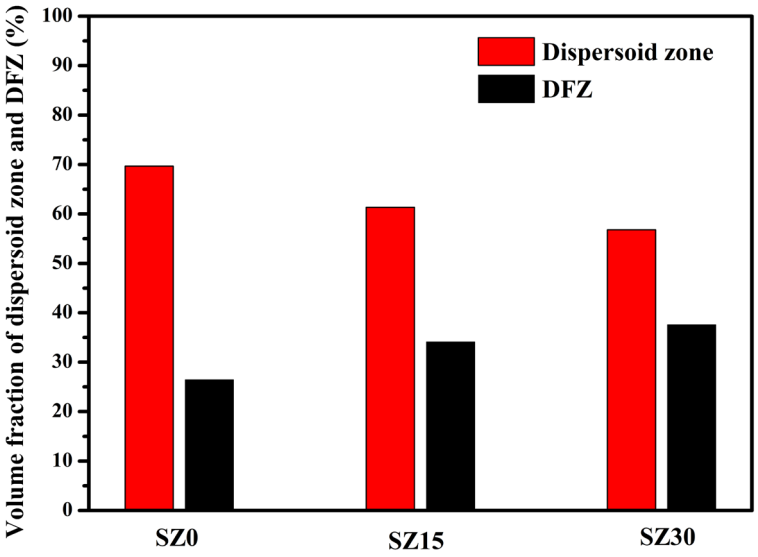

Fig. 4 Volume fraction of the dispersoid zone and DFZ of three alloys after heat treatment at 375°C/24h

3.2 Precipitation of α-Al(Mn,Fe)Si dispersoids and Al_3(Sc,Zr) precipitates

Due to the small size of the Al_3(Sc,Zr) precipitates and α-Al(Mn,Fe)Si dispersoids, TEM was used to investigate the precipitation of both Al_3(Sc,Zr) and α-Al(Mn,Fe)Si in aluminum matrices. After heat treatment at 375°C for 24 h, a number of α-Al(Mn,Fe)Si dispersoids precipitated within the aluminum cells and grains; typical TEM images are shown in Fig. 5. The size and number density of dispersoids were quantified by image analysis on TEM images, as shown in Fig. 6a. In the base alloy (SZ0 without Sc and Zr), the sizes of α-Al(Mn,Fe)Si dispersoids are quite small (in the range of 50 nm) and the number density is high (>1000 μm^{-3}). With increasing Sc and Zr content, the size of the α-Al(Mn,Fe)Si dispersoids increased while their number density decreased. For instance, the equivalent diameter of the dispersoids increased from 50 nm (SZ0 Alloy) to 66 nm (SZ15 alloy), and further to 70 nm in the SZ30 alloy. The volume fractions of their dispersoids in the three alloys were calculated according to Eq. 1 and the results are presented in Fig. 6b. The volume fraction of α-Al(Mn,Fe)Si dispersoids in the SZ0 Alloy is 2.69% and it reduced to 1.24% in the SZ15 Alloy and to 1.15% in the SZ30 alloy. It is evident that Sc and Zr addition greatly influences the precipitation of α-Al(Mn,Fe)Si dispersoids, although Sc and Zr do not seem to be the essential elements for the formation of α-Al(Mn,Fe)Si dispersoids. This could be attributed to the fact that the addition of Sc and Zr reduces the solubility of Mn and Si [7, 18] and results in a large amount of intermetallics and a low level of the supersaturated solid solution of Mn and Si after solidification, which are less available for the formation of α-Al(Mn,Fe)Si dispersoids during heat treatment, when compared to the base alloy (SZ0).

To observe Al_3(Sc,Zr) precipitates, centered dark field TEM images were recorded using {100} superlattice reflections of the precipitates along the <110> or <100> zone axis. Typical TEM images of the Al_3(Sc,Zr) precipitates in SZ15 and SZ30 alloys after heat-treatment at 300 °C and 375 °C are shown in Fig. 7. The precipitates can be observed as small bright particles in the TEM images; they are uniformly distributed in the aluminum matrix with high density. The sizes of the Al_3(Sc,Zr) precipitates depends on the heat treatment temperature. When the heat treatment temperature was 300 °C, the diameter of the Al_3(Sc,Zr) precipitates of SZ15 and SZ30 alloys was ~6 nm. As the heat treatment temperature increased to 375 °C,

the diameter of the Al_3(Sc, Zr) precipitates in SZ15 and SZ30 alloys slightly increased to ~8 nm (Fig. 8). According to image analysis, after heat treatment at 375 °C for 24 h, the SZ15 and SZ30 alloys contain approximately 0.24% and 0.30% Al_3(Sc,Zr) precipitates, respectively.

If the dark field TEM images were captured slightly off center of the {100} superlattice reflections of the precipitates, the populations of the two types of strengthening particles, namely α-Al(Mn,Fe)Si dispersoids and Al_3(Sc,Zr) precipitates, can be visualized at the same time. Fig. 9 shows the distribution of α-Al(Mn,Fe)Si dispersoids and Al_3(Sc,Zr) precipitates in the TEM images in the example of the SZ15 alloy. It can be seen that the inter-particle distance in the α-Al(Mn,Fe)Si dispersoids is quite large (in the range of 200 nm) in addition to their relatively large size (Fig. 9a). On the other hand, the Al_3(Sc,Zr) precipitates are much finer and denser in the aluminum matrix than the α-Al(Mn,Fe)Si dispersoids. They filled up the spaces in between large dispersoids (Fig. 9b). Therefore, the inter-particle distances between strengthening particles are dramatically decreased due to the presence of fine Al_3(Sc,Zr) precipitates, resulting in more obstacles for dislocation movement in aluminum cells and grains.

The DFZ along the grain boundaries was also observed by TEM, as shown in Fig. 10. In the bright field image (Fig. 10a), a large DFZ of α-Al(Mn,Fe)Si dispersoids could be observed along the grain boundary. The half-width of the DFZ was calculated to be ~0.67 μm. At the same location, it can been seen in Fig. 10b that Al_3(Sc,Zr) not only appeared in the dispersoid zone but also precipitated in most of the DFZ. There is only a narrow particle free zone near the grain boundary. The half-width of the particle free zone reduced from 0.67 μm to 0.17 μm, which is 4 times lesser than that observed in the presence of α-Al(Mn,Fe)Si dispersoids only.

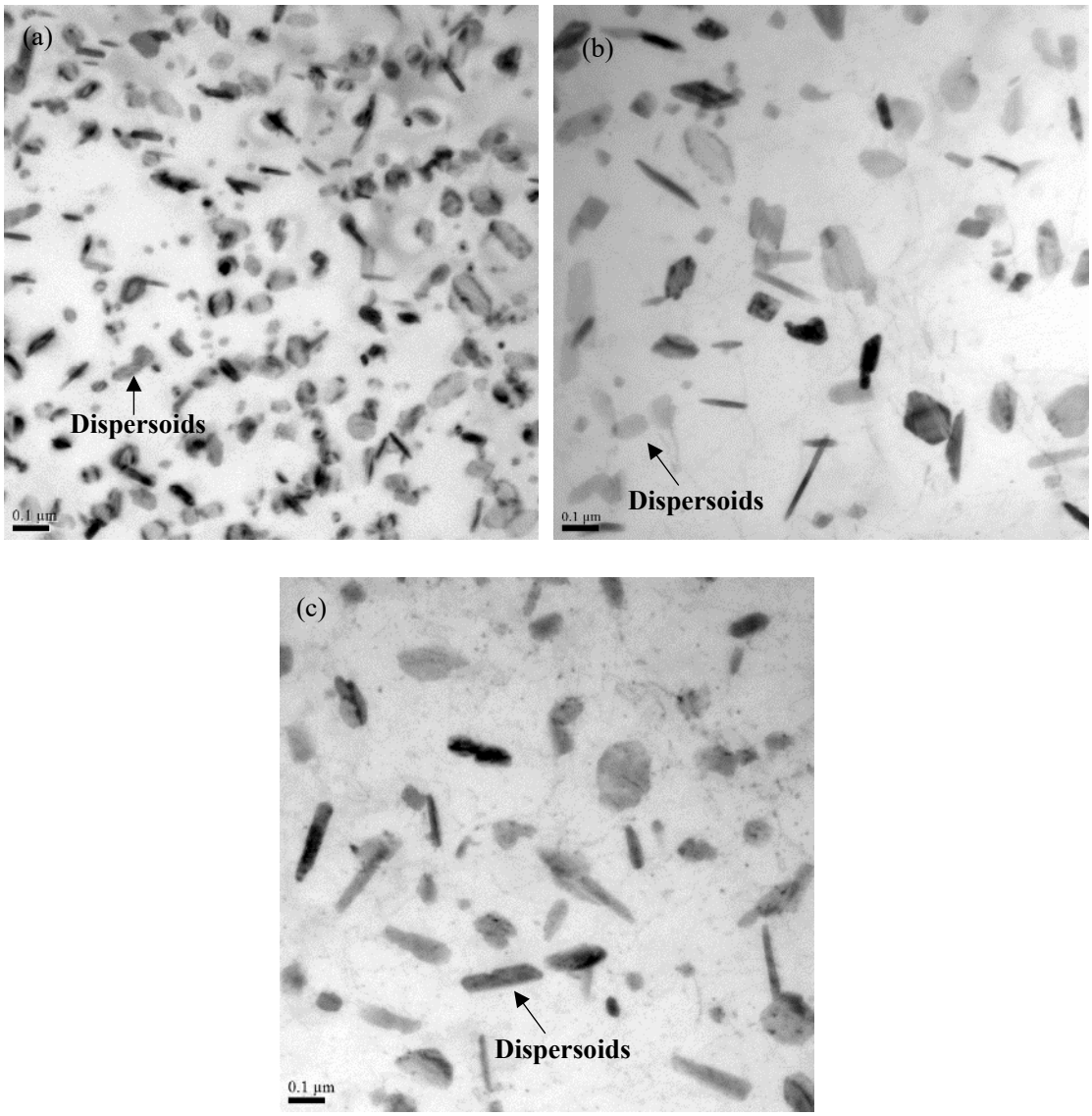

Fig. 5 TEM images of α-Al(Mn,Fe)Si dispersoids (a) SZ0, (b) SZ15 and SZ30 alloys

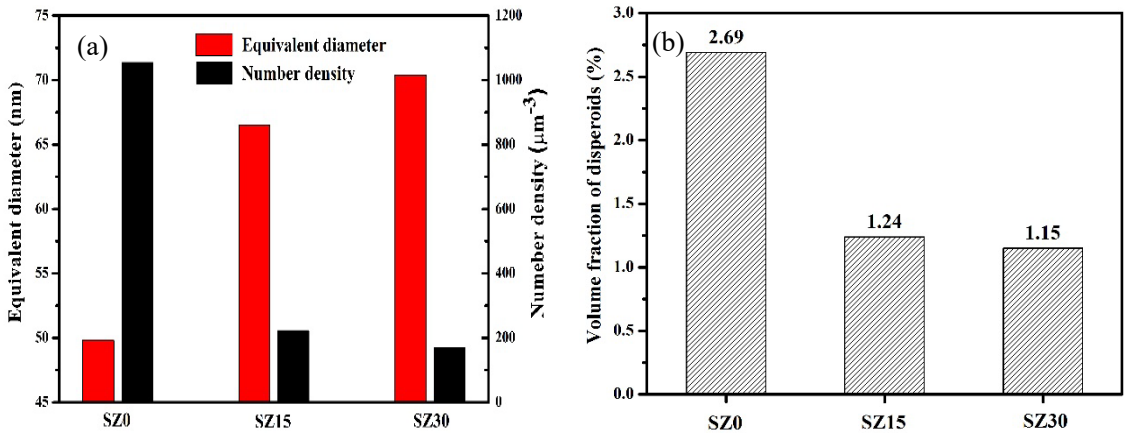

Fig. 6 (a) the equivalent diameter and number density of α-Al(Mn,Fe)Si dispersoids, (b) the volume fraction of α-Al(Mn,Fe)Si dispersoids of three alloys

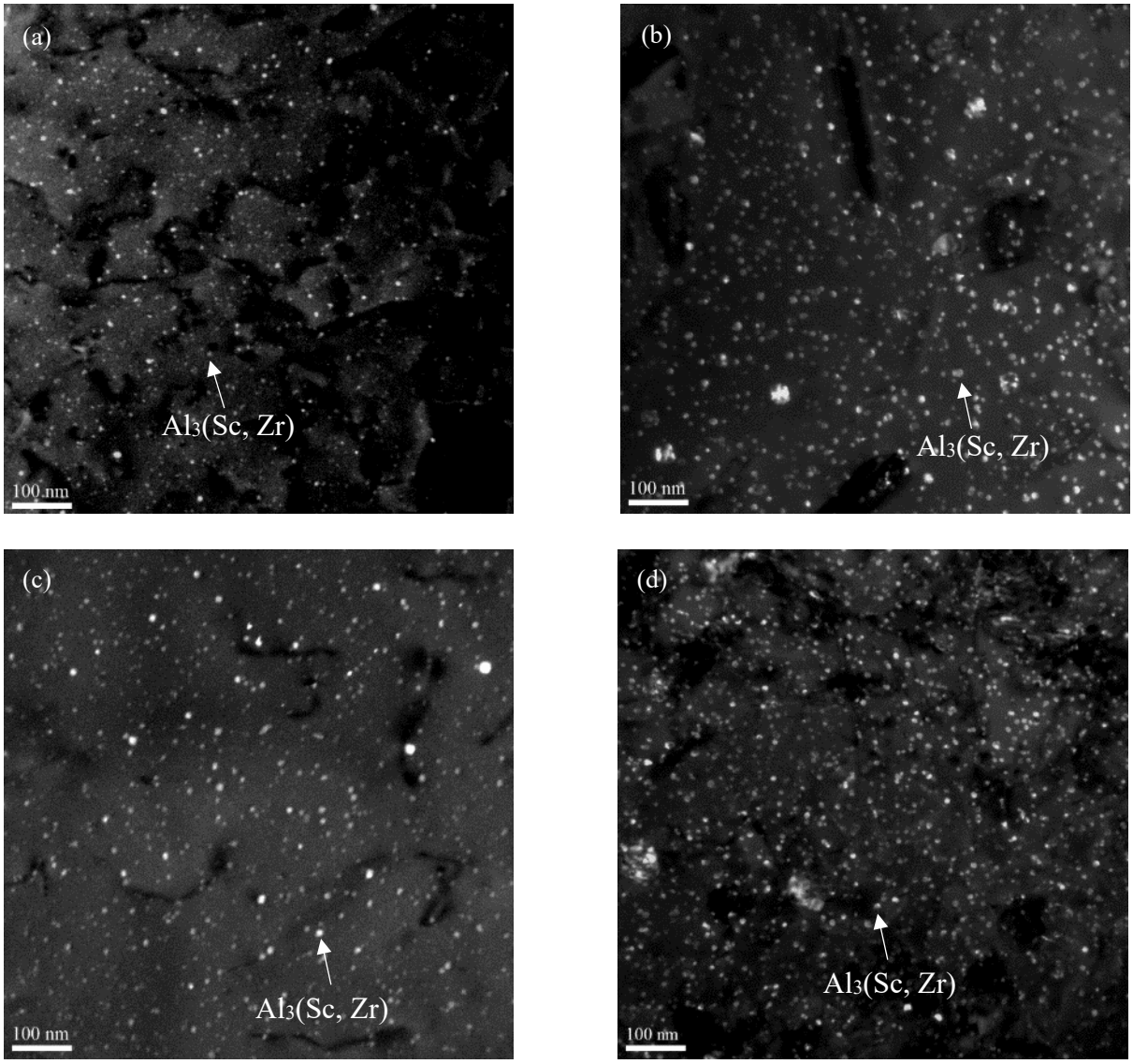

Fig. 7 Centered dark field TEM images of $Al_3(Sc,Zr)$ precipitates (a) SZ15 alloy after 300°C/12h, (b) SZ15 alloy after 375°C/24h, (c) SZ30 alloy after 300°C°/12h, (d) SZ30 alloy after 375°C/24h

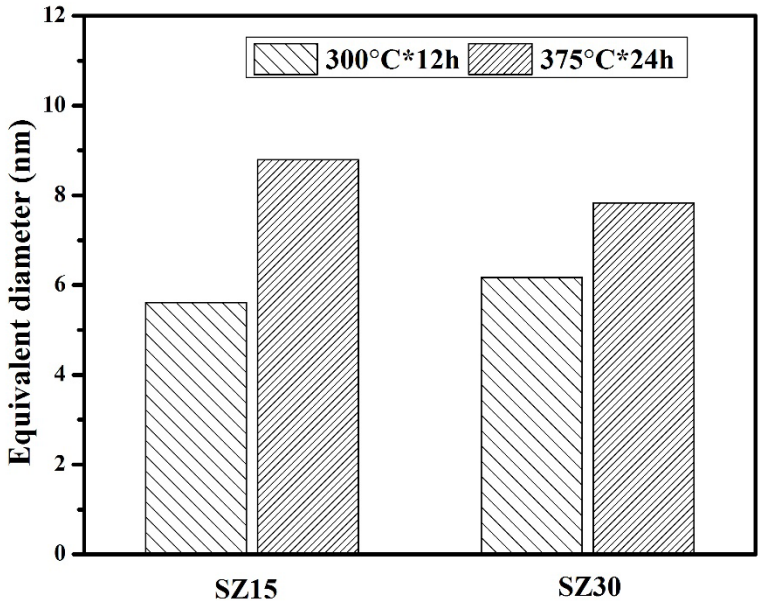

Fig. 8 The equivalent diameter of $Al_3(Sc,Zr)$ precipitates of two alloys at two heat treatment conditions

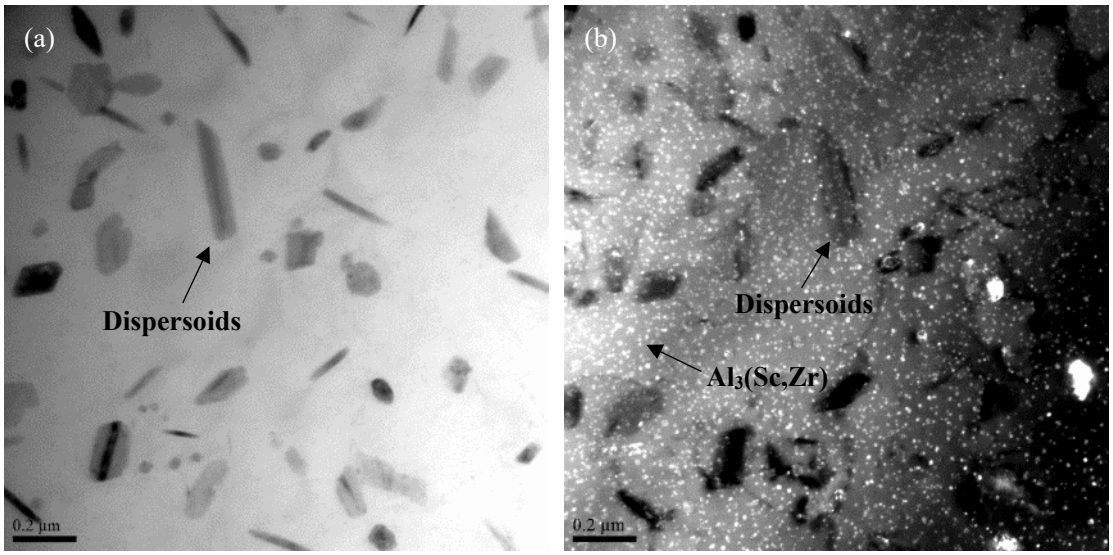

Fig. 9 TEM images showing both α-Al(Mn,Fe)Si dispersoids and $Al_3(Sc,Zr)$ in the aluminum matrix of SZ15 Alloy, (a) bright field TEM image and (b) dark field TEM image captured slightly off the center of {100} superlattice reflections of the $Al_3(Sc,Zr)$ precipitates.

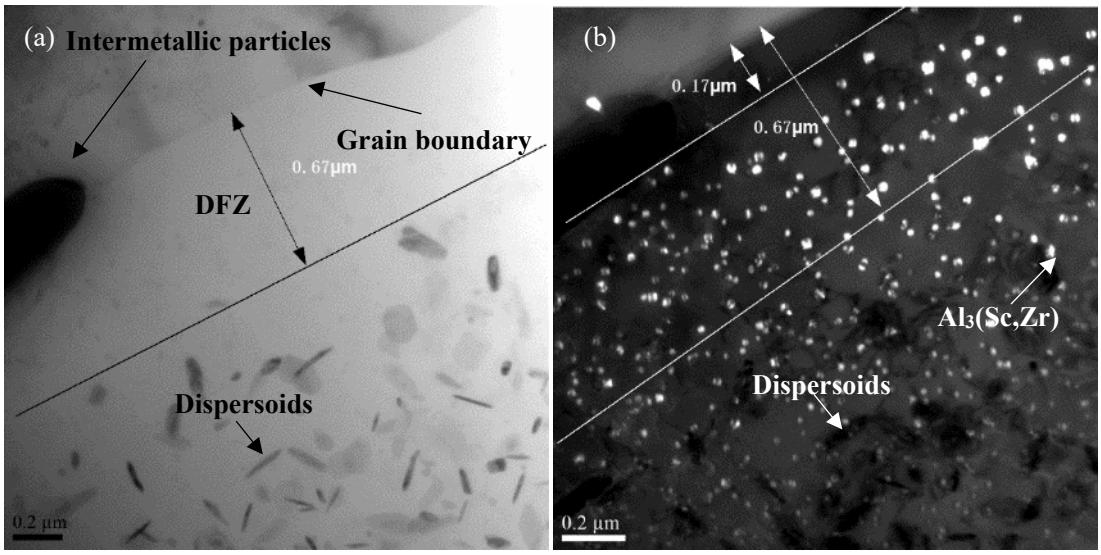

Fig. 10 TEM images of the particle free zone along the grain boundary in SZ15 alloy, (a) bright field TEM image and (b) dark field TEM image captured slightly off the center of {100} superlattice reflections of $Al_3(Sc,Zr)$ precipitates.

3.3 Mechanical properties at ambient and elevated temperatures

3.3.1 Microhardness

To evaluate the influence of Sc and Zr content on the mechanical properties at the ambient temperature, the evolution of microhardness was analyzed in the three alloys after heat treatment at 300 °C and 375 °C (Fig. 11). In the case of the alloys treated at 300 °C (Fig. 11a), the microhardness of the base alloy showed no remarkable change with holding time and remained at a relatively low level because no phase (α-Al(Mn,Fe)Si) precipitation occurred at this temperature. With the addition of Sc and Zr, the hardness of the SZ15 and SZ30 alloys increased with holding time and reached the peak value after 12 h, which indicates the precipitation of $Al_3(Sc,Zr)$, as conformed by the TEM images in Fig. 7. The peak hardness values of SZ0, SZ15 and SZ30 alloys after 300 °C for 12 h are 62, 75 and 81 HV, respectively. The peak hardness of Sc and Zr containing alloys increased by 21% (SZ15) and 31% (SZ30) as compared to the SZ0 base alloy. Because there is no α-Al(M,Fe)Si precipitation in the three alloys, the increase in the hardness of SZ15 and SZ30 alloys is clearly attributed to the strengthening effect of the $Al_3(Sc,Zr)$ precipitates.

In the case of the alloys heat treated at 375 °C (Fig. 11b), the microhardness of the base

alloy increased with holding time and reached the peak value after 24 h, indicating the precipitation of α-Al(Mn,Fe)Si dispersoids. For the Sc and Zr containing alloys, 375 °C is a compatible temperature at which both α-Al(Mn,Fe)Si dispersoids and $Al_3(Sc,Zr)$ preciptates can simultaneously precipitate. The hardness of the SZ15 and SZ30 alloys increased with holding time and reached the peak value after 24 h, indicating the combined precipitation of the two populations of strengthening phases, as conformed by TEM observations in Fig. 9. The peak hardness values of the SZ0, SZ15 and SZ30 alloys after 375 °C for 24 h are 63, 77 and 88 HV, respectively. Due to the addition of Sc and Zr, $Al_3(Sc,Zr)$ precipitates boost the peak hardness by 22% (SZ15) and 40% (SZ30) compared to the base alloy, thus contributing to a considerable fraction of the total hardness, despite a lower volume fraction of the α-Al(Mn,Fe)Si dispersoids in Sc and Zr containing alloys relative to the base alloy (Fig. 6b). This demonstrates that the fine size and high density of $Al_3(Sc,Zr)$ precipitates play a major role in strengthening the aluminum matrix at ambient temperature.

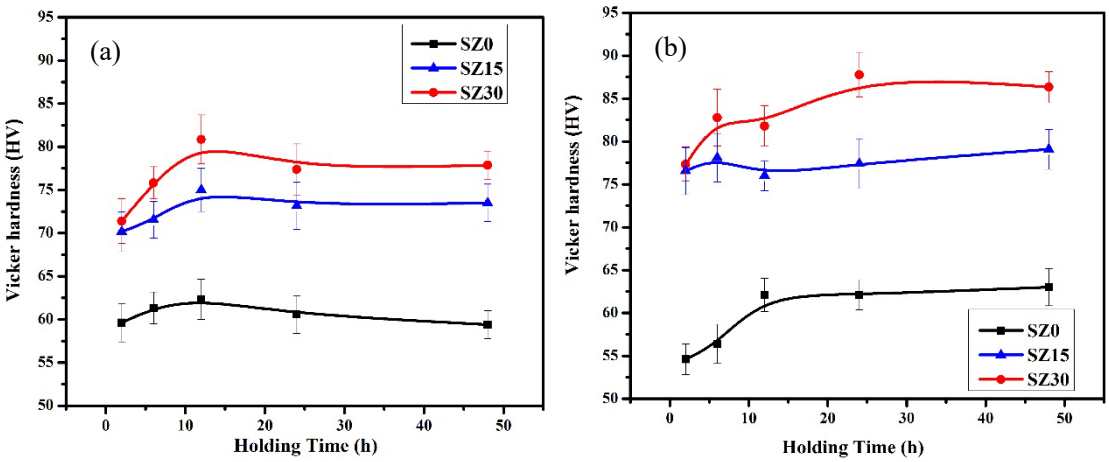

Fig. 11 Microhardness evolution of the three alloys as a function of holding time during heat treatment at (a) 300 °C and (b) 375 °C

3.3.2 Yield strength at ambient and elevated temperatures

The results of yield strength analysis at ambient and elevated temperatures after heat treating the three alloys at 300 °C and 375 °C are shown in Fig. 12. Regardless of the heat treatment temperature, the yield strength at ambient temperature increased greatly with increasing Sc and Zr content (Fig. 12a), which is consistent with the results of peak hardness.

When the alloys treated at 300 °C without α-Al(Mn,Fe)Si precipitation, the yield strength increased from 88 MPa (base alloy) to 130 MPa (SZ15) and further to 135 MPa (SZ30). At a treatment temperature of 375 °C where combined precipitation of α-Al(MnFe)Si dispersoids and Al_3(Sc,Zr) precipitates occurs, the yield strength values of the three alloys are generally higher than that those treated at 300 °C; the yield strength increased from 98 MPa (base alloy) to 135 MPa (SZ15) and further to 154 MPa (SZ30). At both heat treatment conditions, at least more than 37 MPa increase in the yield strength could be achieved with the addition of Sc and Zr, illustrating the potent strengthening effect of Al_3(Sc,Zr) precipitates at the ambient temperature.

The yield strengths at 300 °C exhibit a somewhat different trend from those obtained at the ambient temperature. After heat treatment at 300 °C for 12 h, the yield strength at 300 °C is 62 MPa, 77 MPa and 78 MPa, respectively, for the SZ0, SZ15 and SZ30 alloys (Fig. 12b). They increased approximately by 15 MPa upon the addition of Sc and Zr, whereas the high Sc level in SZ30 showed almost no effect. The strengthening contribution of Al_3(Sc,Zr) precipitates on the yield strength at 300 °C could be clearly seen but it is far less than that at the ambient temperature. In the case of heat treatment at 375 °C for 24 h, the yield strengths of all the three alloys at 300 °C were found to be similar (around 80 MPa) and no remarkable change could be found despite the precipitation of the Al_3(Sc,Zr) in SZ15 and SZ30 alloys. It is noticed that a high density of Al_3(Sc,Zr) precipitated in Sc and Zr containing alloys (SZ15 and SZ30) but the amount of α-Al(Mn,Fe)Si dispersoids in both the alloys are dramatically lower than in the base alloy (see Fig. 6b). The complex effect of these two distinct populations of strengthening particles at ambient and elevated temperatures will be discussed later.

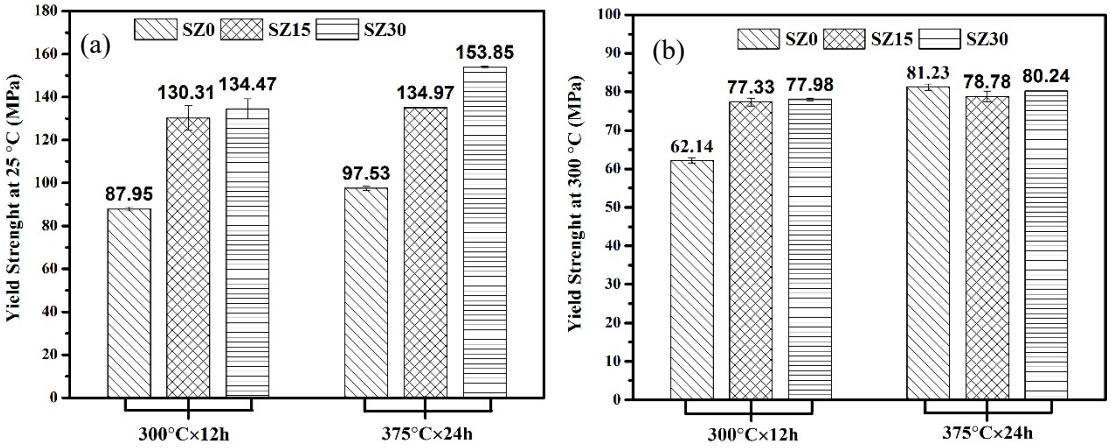

Fig. 12 Yield strengths (a) at 25°C and (b) at 300 °C for two heat treatment conditions

3.3.3 Creep resistance at 300 °C

Fig. 13 shows the typical compressive creep curves of the three alloys tested at 300 °C at a constant load of 58 MPa. It can be found that the total creep strain after 96 h decreased with an increase in the Sc and Zr content. At first, the total creep strain significantly decreased from 0.25 in the SZ0 alloy to 0.10 in the SZ15 alloy and then slightly reduced to 0.09 in the SZ30 alloy, indicating an improvement in the creep resistance by the addition of Sc and Zr. Moreover, the minimum creep rate, $\dot{\varepsilon}_m$, also decreased upon the addition of Sc and Zr. The minimum creep rate is calculated to be 7.58 x 10^{-7} s^{-1} for the base alloy (SZ0); it dropped to 1.69 x 10^{-7} s^{-1} in the SZ15 alloy and then slightly decreased to 1.67 x 10^{-7} s^{-1} in the SZ30 alloy. It is evident that with the addition 0.18%Sc and 0.18%Zr in SZ15, the creep resistance of the material can be significantly enhanced. However, at higher Sc level (0.29% in the SZ30 alloy), the creep resistance improved only slightly.

The creep behavior of dispersion-strengthened materials can generally be described by a modified power law equation [19, 20], in which a thermal threshold stress is assumed and the true stress exponent can be determined:

$$\dot{\varepsilon}_m = A_0\left(\frac{\sigma-\sigma_{th}}{G}\right)^{n_t}\exp\left(-\frac{Q}{RT}\right) \quad (2)$$

Where $\dot{\varepsilon}_m$ is the minimum creep rate, A_0 is constant, σ is the applied stress, σ_{th} is the threshold stress, G was the shear modulus, n_t is the true stress exponent, Q is the activation energy, R is the universal gas constant and T is the absolute temperature.

To better understand the creep behavior of Sc and Zr containing alloys, the creep tests at

different loads were performed to determine two important creep parameters, namely the threshold stress (σ_{th}) and true stress exponent (n_t). The threshold stress σ_{th} is calculated as a stress value as the linear fitted curves corresponding to the minimum creep rates at different loads extrapolated to $1x10^{-10}$ s^{-1} (below which the creep is experimentally not measurable). The true stress exponent n_t is equivalent to the slope of $\ln\dot{\varepsilon}_m$ vs. $\ln(\sigma\text{-}\sigma_{th})$ curve. The calculated results are shown in Fig. 14. As shown in Fig. 14a, the minimum creep rates decreased with the addition of Sc and Zr in the SZ30 alloy at all applied loads; meanwhile the threshold stress σ_{th} increased from 29.1 MPa in the SZ0 alloy to 32.7 MPa in the SZ30 alloy, which is a significant improvement in the creep resistance at elevated temperature. It is reported that an increase of 3 MPa in the threshold stress translates into a decrease in the minimum creep rate by an order of magnitude [21]. Fig. 14b depicts the double logarithmic plots of the minimum creep rate as a function of the effective stress ($\sigma - \sigma_{th}$) along with the slopes of the plots, which yield the values of the true stress exponent. The true stress exponent values of the SZ0 and SZ30 alloys are 5.26 and 5.23, respectively, which suggests that creep is controlled by the high temperature dislocation climb mechanism [20, 22, 23].

Upon appropriate heat treatment (375 °C for 24 h), the precipitation of a number of α-Al(Mn,Fe)Si dispersoids in the 3004 alloy could greatly enhance its creep resistance compared to the conventional 3004 alloy without α-Al(Mn,Fe)Si dispersoids [3]. However, the precipitation of α-Al(Mn,Fe)Si dispersoids is centered in the dendrite cells and grains, leaving a relatively high volume fraction of DFZ in the interdendrite grain boundaries (Fig. 3). The DFZs are weak areas through which the dislocations can easily pass during creep deformation. In addition, a large DFZ in the vicinity of the grain boundary can promote grain boundary rotation and sliding due to the lack of a secondary strengthening phase, leading to a weak resistance to creep deformation. By the addition of Sc and Zr, finer Al_3(Sc,Zr) precipitates of high density not only precipitated in the dendrite grains but also greatly extended to the dispersoid free zones, resulting in a much smaller particle free zone in the vicinity of the grain boundary (Fig. 10). Because the addition of Sc and Zr also causes a remarkable reduction in the volume fraction of α-Al(Mn,Fe)Si dispersoids (Fig. 6b), an increase in the creep resistance in the cores of the dendrite grains would be limited due to the presence of Al_3(Sc,Zr) precipitates. However, the precipitation of Al_3(Sc,Zr) precipitates in

the dispersoid free zone can greatly inhibit dislocation movement as well as grain boundary rotation and sliding, which is considered to be the main factor behind the improved creep resistance of Sc and Zr containing alloys.

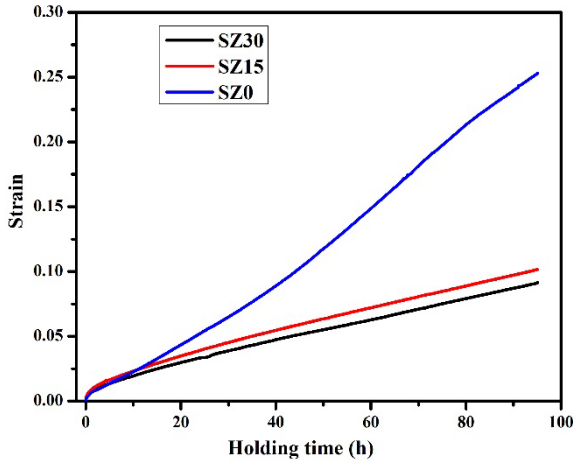

Fig. 13 Typical creep cures of SZ0, SZ15 and SZ30 alloys, conducted at 300 °C for 96 h with a load 58 MPa

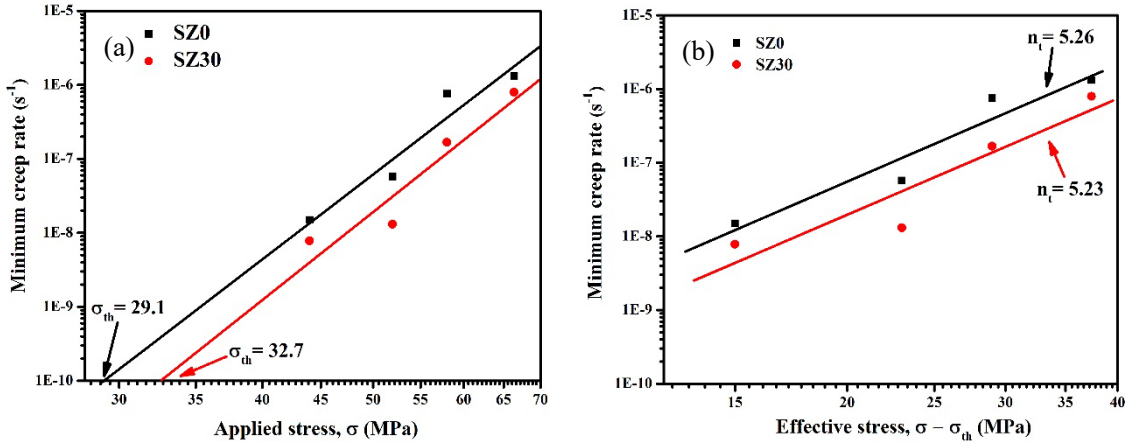

Fig. 14 Logarithmic plots of the minimum creep rate as a function of applied stress to determine the threshold stress σ_{th} (a) and logarithmic plots of the minimum creep rate as a function of effective stress to determine the true stress exponent n_t (b)

3.4 Quantitative analysis of yield strength at ambient and elevated temperatures

To understand the strengthening effect of two distinct populations of particles, α-Al(Mn,Fe)Si dispersoids and $Al_3(Sc,Zr)$ precipitates, at ambient and elevated temperatures,

the yield strengths of the experimental alloys were quantitatively analyzed at 25 °C and at 300 °C. The over yield strength could be considered from several parts, namely the aluminum matrix, solid solution of the alloying elements, α-Al(Mn,Fe)Si dispersoids and $Al_3(Sc,Zr)$ precipitates, and it can be expressed as:

$$\sigma_y = \sigma_m + \Delta\sigma_{SS} + \Delta\sigma_{dispersoids} + \Delta\sigma_{precipitates} \quad (3)$$

where σ_y is the yield strength, σ_m is the matrix strength, $\Delta\sigma_{SS}$ is the strengthening by solid solution, $\Delta\sigma_{dispersoids}$ is the strengthening by α-Al(MnFe)Si dispersoids and $\Delta\sigma_{precipitates}$ is the strengthening by $Al_3(Sc,Zr)$ precipitates. Due to different strengthening mechanisms, the yield strengths at ambient and elevated temperatures are separately discussed.

3.4.1 Yield strength at ambient temperature

The matrix strength (σ_m) is considered to be 34 MPa at 25 °C according to the datasheet of a commercial pure 1100-O aluminum alloy [24]. The solid solution strengthening in the 3004 alloy contributes mainly through Mg and Mn elements and contributions by other elements are almost negligible due to their presence in extremely small quantities. After heat treatment at 375 °C for 24 h, all small Mg_2Si precipitates were assumed to dissolve in the aluminum matrix and the primary Mg_2Si intermetallic particles remained undissolved. At a given volume fraction of primary Mg_2Si intermetallic particles (Fig. 2), the concentrations of Mg in the solid solution of the experimental alloys could be calculated. In the case of Mn, both primary Mn-containing intermetallic particles and α-Al(Mn,Fe)Si dispersoids consumed Mn elements. Based on their volume fractions (Fig. 2 and Fig. 6b), the remaining concentration of Mn in the matrix could be calculated. The results are included in Table 2. The strengthening contribution of Mg and Mn at ambient temperature can be calculated according to Eq. 4 [25, 26]:

$$\Delta\sigma_{SS} = HC^{\alpha} \quad (4)$$

where C was concentration of solute atoms, H_{Mg} = 13.8 MPa/wt%, $\alpha_{Mg} = 1$, H_{Mn} = 18.35 MPa/wt%, $\alpha_{Mn} = 0.9$ [25].

Table 2 Parameters used in the calculation

Alloys	Mg solute content (wt%)	Mn solute content (wt%)	α-Al(Mn,Fe)Si dispersoids		$Al_3(Sc,Zr)$ precipitates	
			Vol.%	Aver. radius (nm)	Vol.%	Aver. radius (nm)
SZ0	0.95	0.17	2.69	25.0	0	0
SZ15	0.84	0.27	1.24	33.2	0.24	4.4
SZ30	0.82	0.14	1.15	35.2	0.30	3.9

For precipitation-strengthened materials, the ambient-temperature strength can be generally explained and predicted using classical Orowan bypass mechanism when the radius of the strengthening particles is greater than 2 nm [27, 28]. In the present work, the radii of the α-Al(Mn,Fe)Si dispersoids and $Al_3(Sc, Zr)$ precipitates are 25-35 nm and 3-4 nm, respectively, which are in the range of the Orowan bypass strengthening mechanism. Therefore, the contribution of both dispersoids and precipitates can be determined using Eq. 5 [2, 6]:

$$\Delta\sigma_{Dispersoids} \text{ or } \Delta\sigma_{precipitates} = \frac{0.84MGb}{2\pi(1-\nu)^{1/2}\lambda} ln\frac{r}{b} \quad (5)$$

$$\lambda = r(\frac{2\pi}{3f})^{1/2} \quad (6)$$

where M = 2 is the Taylor factor [6], G = 27.4 GPa is the shear modulus of Al matrix [6], b = 0.286 nm is the Burgers vector [6], v = 0.33 is the Poison ratio [6], λ is the inter-particle distance, r is the average radius of particles and f is the volume fraction of particles.

The solid solution strengthening of Mg and Mn can be calculated using Eq. (4). Using Eqs. (5) and (6), increments in the yield strength due to the presence of α-Al(Mn,Fe)Si dispersoids and $Al_3(Sc,Zr)$ precipitates are calculated. The calculated results are shown in Table 3 and Fig. 15. It can be seen that solid solution strengthening due to Mg and Mn contributed a relatively small fraction to the strength increment. On the other hand, both α-Al(Mn,Fe)Si dispersoids and $Al_3(Sc,Zr)$ precipitates contributed majorly to the increased strength. In the case of the SZ0 alloy, α-Al(Mn,Fe)Si dispersoids were the only strengthening particles, providing an increment of 52.1 MPa in the yield strength. In the cases of the alloys

with Sc and Zr, two populations of particles existed, and the $Al_3(Sc,Zr)$ precipitates contributed more to the increase in strength compared to the α-Al(Mn,Fe)Si dispersoids. Considering the SZ30 alloy for an example, α-Al(Mn,Fe)Si dispersoids and $Al_3(Sc,Zr)$ precipitates led to 26 MPa and 64.9 MPa increments in strength, respectively. The volume fraction of the α-Al(Mn,Fe)Si dispersoids decreased from 2.69% (SZ0 alloy) to 1.15% (SZ30 alloy) due to the addition of Sc and Zr. Therefore, the yield strength contribution dropped from 52.1 MPa (SZ0 alloy) to 26 MPa (in SZ30 alloy). On the other hand, although the volume fraction of the $Al_3(Sc,Zr)$ precipitates was low, because of their small size and large number density, their strengthening effect was very strong at ambient temperature (64.9 MPa). This is the reason why the yield strength of Sc and Zr containing alloys are higher than that of the base alloy (SZ0). It is evident from Fig. 15 that a good agreement exists between the calculated and experimentally measured results, indicating that the above described analytical solution can be used to predict the yield strength of alloys containing two populations of strengthening phases.

Table 3 The yield strength contributions at 25 °C of each component (MPa)

	SZ0	SZ15	SZ30
Aluminum matrix	34	34	34
Mg solid solution	13.1	11.6	11.3
Mn solid solution	3.7	5.6	3.1
$Al_3(Sc,Zr)$	0	53.9	64.9
α-Al(Mn,Fe)Si	52.1	28.2	26.0
Total of calculated results	102.9	133.3	139.3
Experimental results	97.5	135.0	153.9

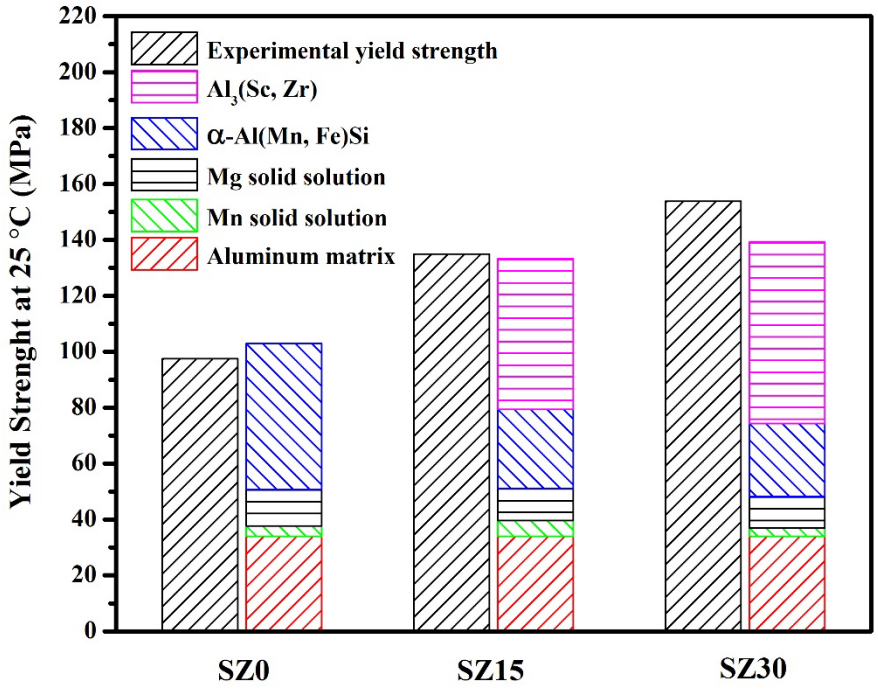

Fig. 15 The comparison between calculated and experimentally measured yield strengths at 25 °C.

3.4.2 Yield strength at 300 °C

It is difficult to estimate the contribution of solid solution strengthening due to Mg and Mn at 300 °C because of the lack of the necessary data on H and α at elevated temperatures in Eq. 4. To solve this problem, the available data on the yield strength of AA3004-O at 315 °C (41 MPa) [29] was used as a close approximation for both the matrix strength and the solid solution strengthening contribution of Mg and Mn at 300 °C.

In the case of the nanometer scale $Al_3(Sc,Zr)$ precipitates, the elevated-temperature strength contribution is difficult to be explained by the classical Orowan bypass mechanism, which often overestimates the atual strength increment [28]. At elevated temperatures, there is sufficient thermal energy to allow dislocation to circumvent the precipitates by climbing over them. The dislocation climb mechanism becomes active when the alloys are deformed at elevated temperatures at low strain rates [30, 31]. Because of the size range of the $Al_3(Sc,Zr)$ precipitates, the dislocation climb mechanism is invoked to better calculate the yield strength contribution of the coherent $Al_3(Sc,Zr)$ precipitates at 300 °C [28]. The increase in strength

due to the dislocation climb ($\Delta\sigma_{Climb}$) consists of two parts, lattice mismatch strengthening ($\Delta\sigma_{LMC}$) and modulus mismatch strengthening ($\Delta\sigma_{MMC}$) which can calculated according to following equations [28, 30]:

$$\Delta\sigma_{Climb} = \Delta\sigma_{LMC} + \Delta\sigma_{MMC} \quad (7)$$

$$\Delta\sigma_{LMC} = \chi(\varepsilon G_m)^{\frac{3}{2}} M \sqrt{\frac{2fbr}{G_m b^2}} \quad (8)$$

$$\Delta\sigma_{MMC} = \frac{F^{\frac{3}{2}} M}{\left(\frac{G_m b^2 2\pi}{3f}\right)^{\frac{1}{2}} br} \quad (9)$$

where, χ = 2.6 was a constant [28, 32], ε was the constrained strain [28, 33], G_m = 21.1 GPa was the shear modulus of Al matrix [28], M = 3.06 was the mean matrix orientation factor [28], b = 0.288 nm was the Burgers vector [28], r was average radius of precipitates, f was volume fraction of precipitates, F was the force on the dislocations [28].

When the particle size of α-Al(Mn,Fe)Si dispersoids is large, the Orowan bypass strengthening mechanism is still valid at elevated temperatures [28]. Therefore, the yield strength contribution of α-Al(Mn,Fe) Si dispersoids at 300 °C can be calculated using Eqs. 5 and 6. The only different parameter is the shear modulus of the Al matrix, G_m, which changes from 27.4 GPa (at 25 °C) to 21.1 GPa (at 300 °C) [28]. Other constants remain unchanged with temperature. Because of the change in G_m, the increase in yield strength due to α-Al(Mn,Fe)Si dispersoids at 300 °C is lower than that at 25 °C for a given volume fraction.

The calculated results of each strengthening contribution are shown in Table 4 and Fig. 16. For the base alloy (SZ0), the strengthening contribution of α-Al(Mn,Fe)Si dispersoids decreased from 52.1 MPa (at 25 °C) to 40.1 MPa (at 300 °C). For the Sc and Zr containing alloys, the strength increments due to α-Al(Mn,Fe)Si dispersoids at 300 °C were 21.7 MPa (SZ15 alloy) and 20 MPa (SZ30 alloy) respectively, which were approximately 20 MPa less than that of the SZ0 alloy due to the reduced volume fraction of the dispersoids. On the other hand, Al_3(Sc,Zr) precipitates led to an increase of 22 MPa in the SZ15 alloy and 23.4MPa in the SZ 30 alloys. These values are much lower than the strength contribution of Al_3(Sc,Zr)

precipitates at the ambient temperature. At higher temperatures, atomic mobility and the number density of the vacancies are very high, and hence the dislocations can easily climb through the $Al_3(Sc,Zr)$ precipitates, resulting in a small increase in the strength. The total strength contributions of α-Al(Mn,Fe)Si dispersoids and $Al_3(Sc,Zr)$ precipitates are approximately 43 MPa in both SZ15 and SZ30 alloys, which is almost equivalent to the strength contribution of α-Al(Mn,Fe)Si dispersoids in the SZ0 alloy. As a result, the overall yield strengths at 300 °C of the base alloy and Sc and Zr containing alloys are almost similar, as shown in Fig. 16. It is evident that the calculated results agree well with the experimentally measured results.

Table 4 The yield strength contributions at 300 °C of each component (MPa)

	SZ0	SZ15	SZ30
Al matrix of AA3004-O	41	41	41
$Al_3(Sc,Zr)$	0	22.0	23.4
α-Al(Mn,Fe)Si	40.1	21.7	20.0
Total calculated results	81.1	84.7	84.4
Experimental results	81.2	78.8	80.2

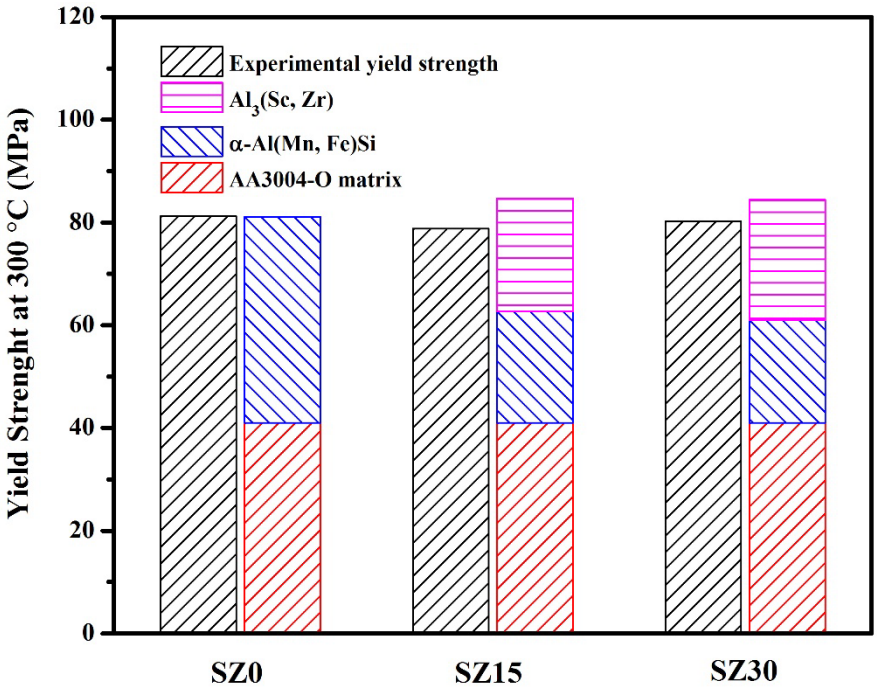

Fig. 16 The comparison between calculated and experimentally measured yield strengths at 300 °C.

3.5 Prospect for the synergetic strengthening effect of co-existing α-Al(Mn,Fe)Si dispersoids and Al_3(Sc,Zr) precipitates

The precipitation and subsequent strengthening mechanisms of α-Al(Mn,Fe)Si dispersoids and Al_3(Sc,Zr) precipitates in Al-Mn-Mg 3004 alloys are quite different due to their differences in morphology, size, volume fraction and distribution. However, for developing strong aluminum alloys with thermal stability for elevated temperature applications, the two strengthening populations can work in complementary manner in many aspects.

(a) Both α-Al(Mn,Fe)Si dispersoids and Al_3(Sc,Zr) precipitates in an aluminum matrix are thermally stable and coarsening resistant at 300-350 °C, which provides a common base for improving the strength and creep resistance at elevated temperatures, as they can effectively impede dislocation glide and climb at the intended service temperature. In addition, the precipitation temperature ranges of α-Al(Mn,Fe)Si dispersoids and Al3(Sc,Zr) precipitates in Al-Mn-Mg 3004 alloys are quite similar. This makes the peak precipitation of both phases during heat treatment feasible.

(b) The amount of Al_3(Sc,Zr) that can be precipitated is rather limited upon alloying with a small quantity of Sc (0.1-0.4%), which makes it suitable only to provide extra strength to the aluminum alloy. On the other hand, a relatively large amount of α-Al(Mn,Fe)Si dispersoids (~3 vol.%) can be precipitated in the conventional low cost Al-Mn-Mg 3004 alloys. Even though the strengthening due to α-Al(Mn,Fe)Si dispersoids is not very effective due to their large size in the submicron scale, their large volume fraction is very good for improving the strength and creep resistance at elevated temperatures [3, 5, 17]. If they can strengthen together in a complementary manner with fine nano-sized Al_3(Sc,Zr), it would greatly reduce the inter-particle spacing and impede dislocation motion, resulting in a great improvement in the mechanical performance of the materials in both ambient and elevated temperatures.

(c) During the precipitation of α-Al(Mn,Fe)Si dispersoids, there is always a relatively large amount of an accompanying dispersoid free zone, which limits improvement in the strength and creep resistance. The uniform distribution of Al_3(Sc,Zr) precipitates in the aluminum matrix, including in the dispersoid free zone, solves this problem perfectly, leading to further improvement in the strength and creep resistance of the material.

(d) In the present work, although the Sc content of the SZ30 alloy is 40% higher than that of the SZ15 alloy, the improvement margin in the yield strength and creep resistance of the high Sc alloy (SZ30) is much smaller than that of the low Sc alloy (SZ15) versus the Sc-free base alloy. Due to the high price of Sc, low Sc alloys (0.1-0.2%) are to be developed because of their cost effective nature; they exhibita synergetic strengthening effect owing to both α-Al(Mn,Fe)Si dispersoids and Al_3(Sc,Zr) precipitates.

(e) In the present work, it is found that the addition of Sc and Zr considerably reduces the amount of α-Al(Mn,Fe)Si dispersoids precipitated in Al-Mn-Mg 3004 alloys. If this problem can be solved in the future, an excellent synergetic strengthening effect due to both phases can be expected.

4. Conclusions

The present work investigated the microstructure, mechanical properties and creep resistance of dispersion-strengthened Al-Mn-Mg 3004 alloy containing two populations of strengthening particles: 50-70 nm-sized α-Al(Mn,Fe)Si dispersoids and 6-8 nm-sized Al_3(Sc,Zr) precipitates. The following conclusions could be drawn.

1. With increasing Sc and Zr contents, the amount of Mn-containing intermetallics and primary Mg_2Si particles increased in the as-cast microstructure of the 3004 alloy.
2. With the addition of Sc and Zr, two populations of strengthening particles (α-Al(Mn,Fe)Si dispersoids and Al_3(Sc,Zr) precipitates) were formed in the 3004 alloy after heat treatment at 375 °C for 24 h. Both the populations contributed to the mechanical properties and creep resistance at ambient and elevated temperatures.
3. The volume fraction of the α-Al(Mn,Fe)Si dispersoids decreased while the volume fraction of the dispersoid free zone increased with increasing Sc and Zr content.
4. The microhardness and yield strength at the ambient temperature greatly increased while

the yield strength at 300 °C did not vary even though the Sc and Zr content increased.

5. The addition of Sc and Zr significantly improved the creep resistance at 300 °C due to the precipitation of fine $Al_3(Sc,Zr)$ and reduction of the particle free zone.
6. The combined effects of α-Al(Mn,Fe)Si dispersoids and $Al_3(Sc,Zr)$ precipitates on the yield strengths at 25 °C and 300 °C were quantitatively analyzed based on the Orowan bypass and dislocation climb mechanisms. The analytically predicted yield strengths were in good agreement with the experimental observations.

Acknowledgments

The authors would like to acknowledge the financial support of the Natural Sciences and Engineering Research Council of Canada (NSERC) and Rio Tinto Aluminum through the NSERC Industry Research Chair in the Metallurgy of Aluminum Transformation at University of Quebec at Chicoutimi.

References

1. Y. J. Li, L. Arnberg, Quantitative study on the precipitation behavior of dispersoids in DC-cast AA3003 alloy during heating and homogenization, Acta Materialia. 51 (2003) 3415-3428. Doi: http://dx.doi.org/10.1016/S1359-6454(03)00160-5.
2. A. M. F. Muggerud, E. A. Mørtsell, Y. Li, R. Holmestad, Dispersoid strengthening in AA3xxx alloys with varying Mn and Si content during annealing at low temperatures, Materials Science and Engineering: A. 567 (2013) 21-28. Doi: http://dx.doi.org/10.1016/j.msea.2013.01.004.
3. K. Liu, X. G. Chen, Development of Al–Mn–Mg 3004 alloy for applications at elevated temperature via dispersoid strengthening, Materials & Design. 84 (2015) 340-350. Doi: http://dx.doi.org/10.1016/j.matdes.2015.06.140.
4. Z. Li, Z. Zhang, X. G. Chen, Effect of magnesium on dispersoid strengthening of Al—Mn—Mg—Si (3xxx) alloys, Transactions of Nonferrous Metals Society of China. 26 (2016) 2793-2799. Doi: http://dx.doi.org/10.1016/S1003-6326(16)64407-2.

5. K. Liu, X.-G. Chen, Evolution of Intermetallics, Dispersoids, and Elevated Temperature Properties at Various Fe Contents in Al-Mn-Mg 3004 Alloys, Metallurgical and Materials Transactions B. 47 (2016) 3291-3300. Doi: http://dx.doi.org/10.1007/s11663-015-0564-y.

6. Y. J. Li, A. M. F. Muggerud, A. Olsen, T. Furu, Precipitation of partially coherent α-Al(Mn,Fe)Si dispersoids and their strengthening effect in AA 3003 alloy, Acta Materialia. 60 (2012) 1004-1014. Doi: http://dx.doi.org/10.1016/j.actamat.2011.11.003.

7. E. A. Marquis, D. N. Seidman, Coarsening kinetics of nanoscale Al3Sc precipitates in an Al–Mg–Sc alloy, Acta Materialia. 53 (2005) 4259-4268. Doi: https://doi.org/10.1016/j.actamat.2005.05.025.

8. E. A. Marquis, D. N. Seidman, Nanoscale structural evolution of Al3Sc precipitates in Al(Sc) alloys, Acta Materialia. 49 (2001) 1909-1919. Doi: https://doi.org/10.1016/S1359-6454(01)00116-1.

9. G. M. Novotny, A. J. Ardell, Precipitation of Al3Sc in binary Al–Sc alloys, Materials Science and Engineering: A. 318 (2001) 144-154. Doi: https://doi.org/10.1016/S0921-5093(01)01326-0.

10. C. Fuller, J. Murray, D. Seidman, Temporal evolution of the nanostructure of Al(Sc,Zr) alloys: Part I – Chemical compositions of Al(ScZr) precipitates, Acta Materialia. 53 (2005) 5401-5413. Doi: https://doi.org/10.1016/j.actamat.2005.08.016

11. J. Lai, Z. Zhang, X. G. Chen, The thermal stability of mechanical properties of Al–B4C composites alloyed with Sc and Zr at elevated temperatures, Materials Science and Engineering: A. 532 (2012) 462-470. Doi: https://doi.org/10.1016/j.msea.2011.11.013.

12. C. Fuller, D. Seidman, Temporal evolution of the nanostructure of Al(Sc,Zr) alloys: Part II-coarsening of Al(ScZr) precipitates, Acta Materialia. 53 (2005) 5415-5428. Doi: https://doi.org/10.1016/j.actamat.2005.08.015

13. P. Naga Raju, K. Srinivasa Rao, G. M. Reddy, M. Kamaraj, K. Prasad Rao, Microstructure and high temperature stability of age hardenable AA2219 aluminium alloy modified by Sc, Mg and Zr additions, Materials Science and Engineering: A.

464 (2007) 192-201. Doi: https://doi.org/10.1016/j.msea.2007.01.144.

14. P. Cavaliere, M. Cabibbo, Effect of Sc and Zr additions on the microstructure and fatigue properties of AA6106 produced by equal-channel-angular-pressing, Materials Characterization. 59 (2008) 197-203. Doi: https://doi.org/10.1016/j.matchar.2006.12.013.

15. Y. Deng, Z. Yin, K. Zhao, J. Duan, Z. He, Effects of Sc and Zr microalloying additions on the microstructure and mechanical properties of new Al–Zn–Mg alloys, Journal of Alloys and Compounds. 530 (2012) 71-80. Doi: https://doi.org/10.1016/j.jallcom.2012.03.108.

16. J. Lai, Z. Zhang, X. G. Chen, Precipitation strengthening of Al–B4C metal matrix composites alloyed with Sc and Zr, Journal of Alloys and Compounds. 552 (2013) 227-235. Doi: http://doi.org/10.1016/j.jallcom.2012.10.096.

17. Z. Li, Z. Zhang, X. G. Chen, Microstructure, elevated-temperature mechanical properties and creep resistance of dispersoid-strengthened Al-Mn-Mg 3xxx alloys with varying Mg and Si content, Materials Science and Engineering: A. 708 (2017) 383-394. Doi: http://dx.doi.org/10.1016/j.msea.2017.10.013.

18. L. L. Rokhlin, N. R. Bochvar, I. E. Tarytina, N. P. Leonova, Phase composition and recrystallization of Al-based Al-Sc-Mn-Zr alloys, Russian Metallurgy (Metally). 2010 (2010) 241-247. Doi: http://dx.doi.org/10.1134/S0036029510030158.

19. R. A. Karnesky, L. Meng, D. C. Dunand, Strengthening mechanisms in aluminum containing coherent Al3Sc precipitates and incoherent Al2O3 dispersoids, Acta Materialia. 55 (2007) 1299-1308. Doi: http://dx.doi.org/10.1016/j.actamat.2006.10.004.

20. L. Pan, K. Liu, F. Breton, X. -Grant Chen, Effect of Fe on Microstructure and Properties of 8xxx Aluminum Conductor Alloys, Journal of Materials Engineering and Performance. 25 (2016) 5201-5208. Doi: http://dx.doi.org/10.1007/s11665-016-2373-0.

21. A. R. Farkoosh, X. Grant Chen, M. Pekguleryuz, Interaction between molybdenum and manganese to form effective dispersoids in an Al–Si–Cu–Mg alloy and their influence on creep resistance, Materials Science and Engineering: A. 627 (2015)

127-138. Doi: http://dx.doi.org/10.1016/j.msea.2014.12.115.

22. F. A. Mohamed, K.-T. Park, E. J. Lavernia, Creep behavior of discontinuous SiC Al composites, Materials Science and Engineering: A. 150 (1992) 21-35. Doi: http://dx.doi.org/10.1016/0921-5093(90)90004-M.

23. Y. Li, T. G. Langdon, An examination of a substructure-invariant model for the creep of metal matrix composites, Materials Science and Engineering: A. 265 (1999) 276-284. Doi: http://dx.doi.org/10.1016/S0921-5093(98)01131-9.

24. J. G. Kaufman, Properties of Aluminum Alloys: Tensile, Creep, and Fatigue Data at High and Low Temperatures. (ASM international, 1999), pp. 9.

25. E. L. Huskins, B. Cao, K. T. Ramesh, Strengthening mechanisms in an Al–Mg alloy, Materials Science and Engineering: A. 527 (2010) 1292-1298. Doi: http://dx.doi.org/10.1016/j.msea.2009.11.056.

26. Ø. Ryen, B. Holmedal, O. Nijs, E. Nes, E. Sjölander, H.-E. Ekström, Strengthening mechanisms in solid solution aluminum alloys, Metallurgical and Materials Transactions A. 37 (2006) 1999-2006. Doi: http://dx.doi.org/10.1007/s11661-006-0142-7.

27. C. B. Fuller, D. N. Seidman, D. C. Dunand, Mechanical properties of Al(Sc,Zr) alloys at ambient and elevated temperatures, Acta Materialia. 51 (2003) 4803-4814. Doi: https://doi.org/10.1016/S1359-6454(03)00320-3.

28. J. Qin, Z. Zhang, X.-G. Chen, Mechanical Properties and Strengthening Mechanisms of Al-15 Pct B4C Composites with Sc and Zr at Elevated Temperatures, Metallurgical and Materials Transactions A. 47 (2016) 4694-4708. Doi: http://dx.doi.org/10.1007/s11661-016-3606-4.

29. J. G. Kaufman, Properties of Aluminum Alloys: Tensile, Creep, and Fatigue Data at High and Low Temperatures. (ASM international, 1999), pp. 102.

30. E. A. Marquis, D. C. Dunand, Model for creep threshold stress in precipitation-strengthened alloys with coherent particles, Scrita Materialia. 47 (2002) 503-508.

31. R.W. Cahn and P. Haasen: Physical Metallurgy, 4th ed., North Holland, The Netherlands, 1996.

32. A. J. Ardell, Precipitation hardening, Metallurgical Transactions A. 16 (1985) 2131-2165. Doi: http://dx.doi.org/10.1007/BF02670416.

33. D. N. Seidman, E. A. Marquis, D. C. Dunand, Precipitation strengthening at ambient and elevated temperatures of heat-treatable Al(Sc) alloys, Acta Materialia. 50 (2002) 4021-4035. Doi: http://dx.doi.org/10.1016/S1359-6454(02)00201-X.